

## IMAGERIE ACOUSTIQUE ET OPTIQUE DES MILIEUX BIOLOGIQUES *OPTICAL AND ACOUSTICAL IMAGING OF BIOLOGICAL MEDIA*

# Optical coherence tomography

James G. FUJIMOTO

Department of Electrical Engineering and Computer Science and Research Laboratory of Electronics,  
Massachusetts Institute of Technology, Cambridge, MA 02139, USA

(Reçu le 6 juillet 2001, accepté le 11 juillet 2001)

---

**Abstract.** Optical Coherence Tomography (OCT) is a new technology for performing high-resolution cross sectional imaging. OCT is analogous to ultrasound imaging, except that it uses light instead of sound. OCT can provide cross sectional images of tissue structure on the micron scale in situ and in real time. OCT functions as a type of optical biopsy and is a powerful imaging technology for medical diagnostics because unlike conventional histopathology which requires removal of a tissue specimen and processing for microscopic examination, OCT can provide images of tissue in situ and in real time. OCT can be used where standard excisional biopsy is hazardous or impossible, to reduce sampling errors associated with excisional biopsy, and to guide interventional procedures. © 2001 Académie des sciences/Éditions scientifiques et médicales Elsevier SAS

**OCT / tomography / optical biopsy / biological tissues**

### *Tomographie de cohérence optique*

**Résumé.** La tomographie de cohérence optique (OCT) est une nouvelle technique pour obtenir des coupes à haute résolution. L'OCT est l'analogie de l'imagerie ultrasonore si ce n'est qu'elle utilise de la lumière à la place des sons. L'OCT est capable de fournir des images en coupes de la structure des tissus, in situ, en temps réel. L'OCT joue le rôle d'une biopsie optique et constitue une méthode puissante d'imagerie pour le diagnostic médical. En effet, à la différence de l'histopathologie conventionnelle qui impose l'ablation d'un échantillon de tissu et sa préparation pour l'examen microscopique, l'OCT peut fournir des images des tissus, in situ et en temps réel. L'OCT peut être utilisée dans des cas où la biopsie par excision est dangereuse ou impossible, pour réduire les erreurs d'échantillonnage de cette biopsie et pour guider les interventions. © 2001 Académie des sciences/Éditions scientifiques et médicales Elsevier SAS

**OCT / tomographie / biopsie optique / tissus biologiques**

---

## 1. Introduction

Optical coherence tomography (OCT) is an emerging optical imaging technology that performs high-resolution, cross-sectional tomographic imaging of internal structure in biological systems and materials [1]. OCT is analogous to ultrasound B mode imaging except that it uses light instead of sound. Image resolutions of 1–15  $\mu\text{m}$  can be achieved, over one order of magnitude higher than conventional ultrasound. OCT performs imaging by measuring the echo time delay and intensity of backscattered light from internal microstructure in the tissue. In biomedicine, OCT can function as a type of optical biopsy,

---

Note présentée par Guy LAVAL.

S1296-2147(01)01257-4/FLA

© 2001 Académie des sciences/Éditions scientifiques et médicales Elsevier SAS. Tous droits réservés

yielding information on tissue pathology in situ and in real time, without the need for excision of specimens and processing as in conventional biopsy and histopathology [2–4].

**2. Principles of operation**

OCT is analogous to ultrasound imaging but uses light instead of sound. Cross-sectional images are generated by measuring the echo time delay and intensity of light that is reflected or backscattered from internal structures in tissue [1]. Because the velocity of light is extremely high, the echo time delay cannot be measured directly. Instead, it is necessary to use correlation or interferometry techniques. One method for measuring the echo time delay of light is to use low-coherence interferometry. Low-coherence interferometry was first developed for measuring reflections in fiber optics and optoelectronic devices [5–7]. The first applications of low-coherence interferometry in biomedicine were in ophthalmology to perform precision measurements of axial eye length and corneal thickness [8,9].

Low-coherence interferometry measures the echo time delay and intensity of backscattered light by interfering it with light that has traveled a known reference path length and time delay. Measurements are performed using a Michelson-type interferometer (*figure 1*). Light from a source is directed onto a beam splitter, and one of the beams is incident onto the sample to be imaged, while the second beam travels a reference path with a variable path length. The backscattered light from the sample is interfered with reflected light from the reference arm and detected with a photodetector at the interferometer output. If the light source is coherent, then interference fringes will be observed as the relative path lengths are varied. However, if low-coherence light or short pulses are used, then interference occurs only when the two path lengths match to within the coherence length of the light. The echo time delay and intensity of backscattered

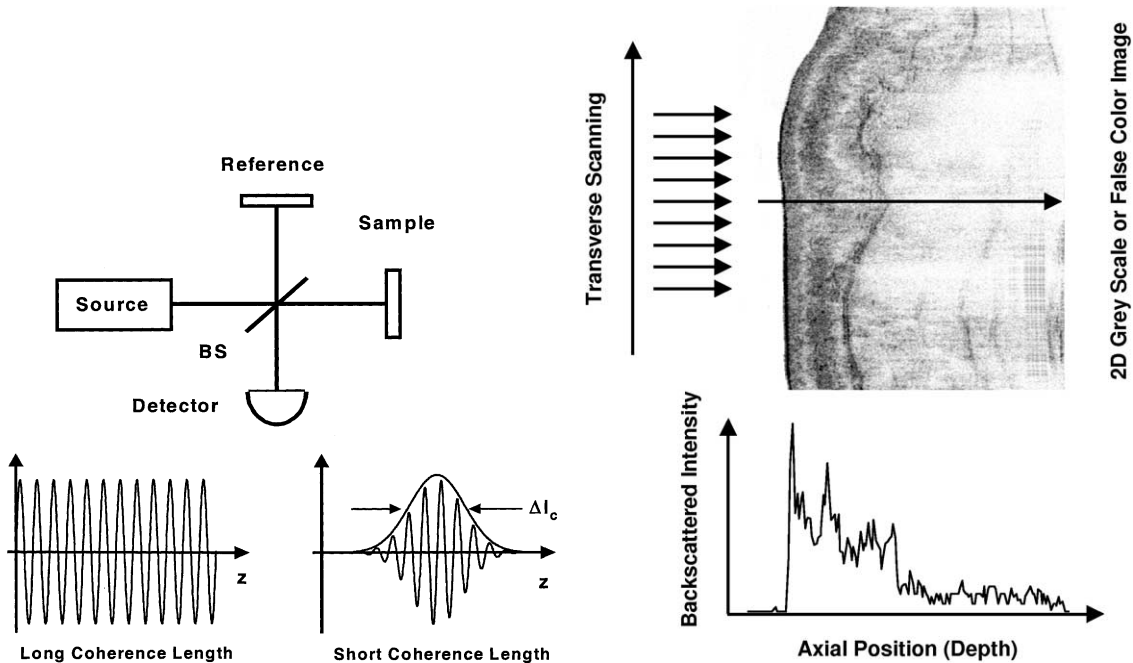


**Figure 1.** OCT measures the echo time delay of reflected light by using low-coherence interferometry. The system is based on a Michelson-type interferometer. Reflections or backscattering from the object being imaged are correlated with light which travels a reference path.

**Figure 2.** Cross-sectional images are constructed by performing measurements of the echo time delay of light at different transverse positions. The result is a two-dimensional data set that represents the backscattering in a cross-sectional plane of the tissue.

light from sites within the sample can be measured by detecting and demodulating the interference output of the interferometer while scanning the reference path length. This method is analogous to heterodyne optical detection in optical communications.

*Figure 2* is a schematic illustrating how OCT performs cross-sectional imaging. The optical beam is focused into the sample being imaged, and the echo time delay and intensity of the backscattered light are measured to yield an axial backscattering profile. The incident beam is then scanned in the transverse direction, and the axial backscattering profile is measured at several transverse positions to yield a two-dimensional data set. This data set represents the optical backscattering through a cross section of the tissue. The data is displayed as a logarithmic gray scale or false color image.

In contrast to conventional microscopy, the mechanisms that govern the axial and transverse image resolution in OCT are independent. The axial resolution in OCT is determined by the coherence length of the light source. Thus high resolution can be achieved independent of the beam focusing conditions. The interference signal from the interferometer is the electric-field autocorrelation of the light source. The coherence length is the spatial width of this field autocorrelation. In addition, the envelope of the field autocorrelation is equivalent to the Fourier transform of the power spectrum. Thus, the width of the autocorrelation function, or the axial resolution, is inversely proportional to the width of the power spectrum. For a source with a Gaussian spectral distribution, the axial resolution  $\Delta z$  is:

$$\Delta z = (2 \ln 2 / \pi) (\lambda^2 / \Delta \lambda)$$

where  $\Delta z$  and  $\Delta \lambda$  are the full-widths-at-half-maximum of the autocorrelation function and power spectrum respectively, and  $\lambda$  is the source center wavelength. The axial resolution is inversely proportional to the bandwidth of the light source, and high resolution may be achieved by using broad bandwidth optical sources.

The transverse resolution in the OCT imaging system is determined by the focused spot size as in conventional microscopy. The transverse resolution is:

$$\Delta x = (4\lambda/\pi)(f/d)$$

where  $d$  is the spot size on the objective lens and  $f$  is its focal length. High transverse resolution can be obtained by using a large numerical aperture and focusing the beam to a small spot size. In addition, the transverse resolution is also related to the depth of focus or the confocal parameter  $b$  which is  $2z_R$ , two times the Raleigh range:

$$2z_R = \pi \Delta x^2 / 2\lambda$$

Improving the transverse resolution produces a decrease in the depth of focus, similar to conventional microscopy.

Finally, the signal to noise of detection can be calculated using standard techniques from optical communications theory and is given by:

$$SNR = 10 \log(\eta P / 2h\nu NEB)$$

where  $P$  is the detected power,  $NEB$  is the noise equivalent bandwidth of the detection,  $\eta$  is the detector quantum efficiency, and  $h\nu$  is the photon energy. The signal to noise ratio scales as the reflected or backscattered power divided by the noise equivalent bandwidth of the detection. Higher image acquisition speeds or higher image resolutions require higher optical powers to achieve a given signal to noise ratio.

One of the advantages of OCT is that it can be implemented using compact fiber optic components and integrated with a wide range of medical instruments. *Figure 3* shows a schematic of an OCT system using fiber optic Michelson-type interferometer. A low-coherence light source is coupled into the interferometer,

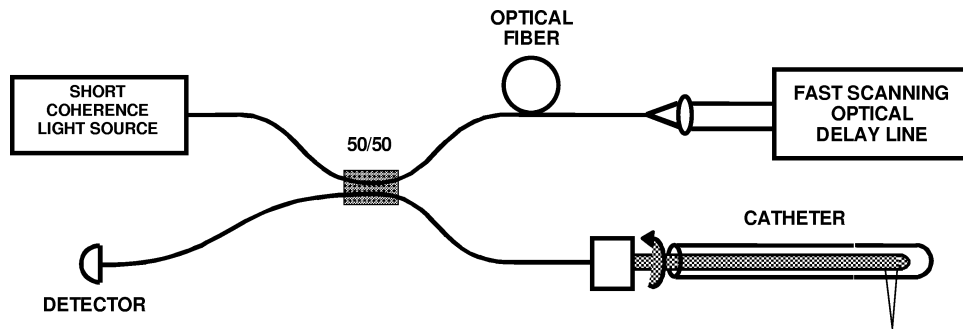


**Figure 3.** Schematic of OCT instrument based on a fiber-optic implementation of a Michelson interferometer. One arm of the interferometer is interfaced to the measurement instrument and the other arm has a scanning delay line. The system shown is configured for high-speed catheter/endoscope based imaging.

and the interference at the output is detected with a photodiode. One arm of the interferometer emits a beam that is directed and scanned on the sample that is being imaged, while the other arm of the interferometer is a reference arm with a scanning delay line. The system can be interfaced to microscopes, hand held imaging probes, as well as catheters and endoscopes.

### 3. Biomedical applications

#### 3.1. Ophthalmic imaging

OCT was first applied for imaging of the eye, and to date, OCT has had the largest clinical impact in ophthalmology [10,11]. *Figure 4* shows an example of an OCT image of the normal retina of a human subject [12]. This image is acquired at a wavelength of 800 nm with a 10 μm resolution and is 250 transverse pixels wide. The retinal pigment epithelium and choroid, which is highly vascular, are visible as highly scattering structures in the OCT image. The retinal nerve fiber layer is visible as a scattering layer originating from the optic disk and becoming thinner approaching the fovea. The total retinal thickness as well as the retinal nerve fiber layer thickness can be measured. The OCT image provides a cross sectional view of the retina with unprecedented resolution and allows detailed structures to be differentiated. Although the retina is almost transparent and has extremely low optical backscattering, the high sensitivity of OCT imaging allows extremely weak backscattering features to be visualized.

Numerous clinical studies have been performed to investigate the feasibility of using OCT for the diagnosis and monitoring of retinal diseases such as glaucoma, macular edema, macular hole, central serous chorioretinopathy, age related macular degeneration, epiretinal membranes, optic disc pits, and choroidal

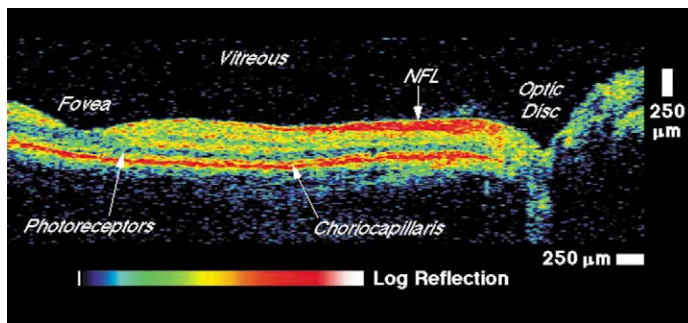


**Figure 4.** OCT image of the human retina papillary-macular axis illustrating the ability to discriminate structural morphology in vivo. The highly backscattering retinal nerve fiber layer (NFL) and choriocapillaris appear red. The optic disk as well as several of the retinal layers are observed. From [12]: Hee M.R. et al., Optical coherence tomography of the human retina, *Arch. Ophthalmol.* 113 (1995) 325–332.

tumors [13–20]. Images can be analyzed quantitatively and processed using intelligent algorithms to extract features such as retinal or retinal nerve fiber layer thickness [16,17]. Mapping and display techniques have been developed to represent the tomographic data in alternate forms, such as thickness maps, in order to aid interpretation [20]. OCT is especially promising for the diagnosis and monitoring of diseases such as glaucoma or diabetic macular edema because it can provide quantitative information about retinal pathology as a measure of disease progression. OCT has the potential to detect and diagnose early stages of disease before physical symptoms and irreversible loss of vision occur.

### 3.2. Optical coherence tomography and optical biopsy

With recent research advances, OCT imaging of optically scattering, nontransparent tissues is possible, thus enabling a wide variety of applications in internal medicine and internal body imaging. One of the most important advances for imaging in optically scattering tissues was the use of longer wavelengths where optical scattering is reduced [2,21–23]. By performing OCT imaging at 1.3  $\mu\text{m}$  wavelengths, image penetration depth of 2 to 3 millimeters can be achieved in most tissues. This imaging depth is comparable to the depth over which many biopsies are performed. In addition, many diagnostically important changes of tissue morphology occur at the epithelial surfaces of organ lumens. The capability to perform in situ and real time imaging could be important in a variety of clinical scenarios including:

- (1) to perform imaging of tissue microstructure in situations where conventional excisional biopsy would be hazardous or impossible;
- (2) to reduce the false negative rates caused by sampling errors of conventional biopsy; and
- (3) to guide surgical or microsurgical intervention.

### 3.3. Imaging where excisional biopsy is hazardous or impossible

One class of applications where OCT is especially promising is where conventional excisional biopsy is hazardous or impossible. In ophthalmology, retinal biopsy cannot be performed, and OCT can provide high-resolution images of pathology that cannot be obtained using any other technique [13–20]. OCT imaging can be performed repeatedly for screening or to monitor disease progression and response to treatment. Another scenario where biopsy is not possible is imaging of atherosclerotic plaque morphology in the coronary arteries [23,24]. Recent research has demonstrated that most myocardial infarctions result from the rupture of small to moderately sized cholesterol-laden coronary artery plaques followed by thrombosis and vessel occlusion. The plaques at highest risk for rupture have a structurally weak fibrous cap. These plaque morphologies are difficult to detect by conventional radiologic techniques, and their microstructural features cannot be determined. *Figure 5* shows an example of an unstable plaque morphology from a human abdominal aorta specimen and corresponding histology. OCT imaging was performed at 1300 nm wavelength using a superluminescent diode light source with an axial resolution of  $\sim 16 \mu\text{m}$ . The OCT image and histology show a small intimal layer covering a large atherosclerotic plaque that is heavily calcified and has a relatively low lipid content. The optical scattering properties of lipid, adipose tissue, and calcified plaque are different and provide contrast between different structures and plaque morphologies. These structures cannot be resolved with ultrasound. Identifying high risk unstable plaques and patients at risk for myocardial infarction is important because of the high percentage of occlusions which result in sudden death. OCT could be a powerful tool for diagnostic intravascular imaging in both risk stratification and guidance of interventional procedures such as atherectomy.

### 3.4. Detecting early neoplastic changes

Another important class of OCT imaging applications is in situations where conventional excisional biopsy has unacceptably high false negative rates due to sampling errors. This situation occurs in the screening and detection of early neoplastic changes. OCT can resolve changes in architectural morphology that are associated with many early neoplastic changes. Numerous in vitro studies have been performed

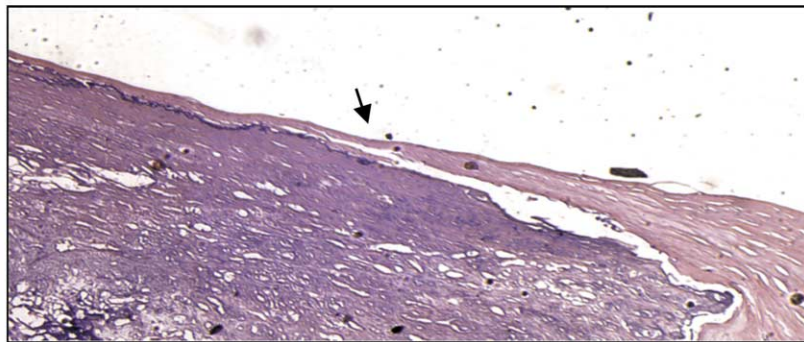
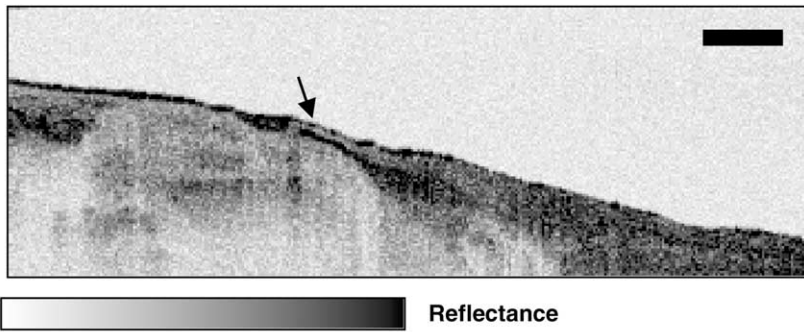


**Figure 5.** In vitro OCT image of atherosclerotic plaque and corresponding histology. The plaque is heavily calcified with a low lipid content. A thin intimal layer covers the plaque. The high resolution of OCT can resolve small structures such as the thin intimal layer that are associated with unstable plaques. The bar is 500  $\mu\text{m}$ . From [23]: Brezinski M.E. et al., Optical coherence tomography for optical biopsy: properties and demonstration of vascular pathology, *Circulation* 93 (1996) 1206–1213.

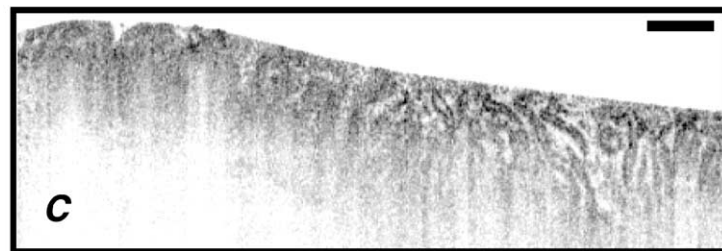
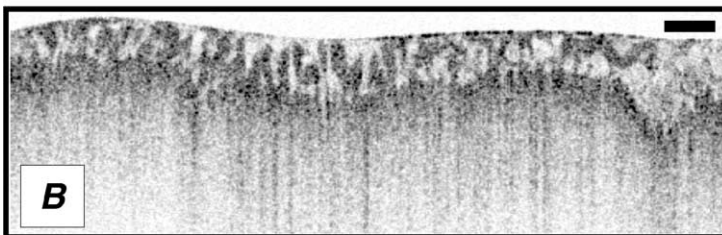
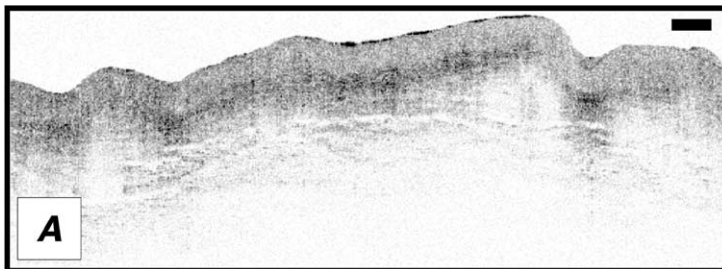


**Figure 6.** In vitro OCT images of human gastrointestinal tissues and pathology. (A) normal human esophagus showing squamous epithelial structure, (B) normal colon with crypt structures, and (C) ampullary carcinoma showing associated disruption of normal epithelial organization. The carcinoma is on the left of the image. These images illustrate the ability of OCT to discriminate architectural morphology relevant to the detection of early neoplastic changes. From [25]: Tearney G.J. et al., Optical biopsy in human gastrointestinal tissue using optical coherence tomography, *Am. J. Gastroent.* 92 (1997) 1800–1804.

to investigate OCT imaging in the gastrointestinal, urinary, respiratory, and female reproductive tracts [25–34]. *Figure 6* shows an example of an OCT image of normal esophagus, normal colon, and ampullary carcinoma. The OCT image of the esophagus shows normal morphology of the mucosa and submucosa. The upper portion of the mucosa appears homogenous in the OCT image and is associated with squamous epithelial architecture. The OCT image of the colon shows normal glandular organization associated with columnar epithelial structure. The mucosa and muscularis mucosa can be differentiated due to the different backscattering characteristics within each layer. Architectural morphology such as crypts or glands within the mucosa can also be seen. Finally, the OCT image of ampullary carcinoma shows disruption of architectural morphology or glandular organization. The area on the right of the image is normal, while the carcinoma is on the left of the image. The crypt structures are dilated and distorted in the middle of the image with complete loss of structure in the carcinoma.

Changes in architectural morphology such as these can be used for the screening and the diagnosis of early neoplastic changes. The imaging depth of OCT is 2–3 mm, less than that of ultrasound. However, for diseases that originate from or involve the mucosa, submucosa, and muscular layers, imaging the microscopic structure of small lesions is well within the range of OCT. Conventional excisional biopsy often suffers from high false negative rates because the biopsy process relies on sampling tissue and the diseased tissues can easily be missed. OCT could be used to identify suspect lesions and to guide excisional biopsy to reduce sampling errors. This would reduce the number of costly biopsies, and at the same time clinical diagnosis could be made using biopsy and histopathology, which is a well established standard. In the future, after more extensive clinical data are available, it may be possible to use OCT directly for the diagnosis or staging of certain types of neoplasias.

### 3.5. Guiding surgical intervention

Another large class of applications for OCT is guiding surgical intervention. The ability to see beneath the surface of tissue in real time can guide surgery near sensitive structures such as vessels or nerves and assist in microsurgical procedures [35–37]. Optical instruments such as surgical microscopes are routinely used to magnify tissue to prevent iatrogenic injury and to guide delicate surgical techniques. OCT can be

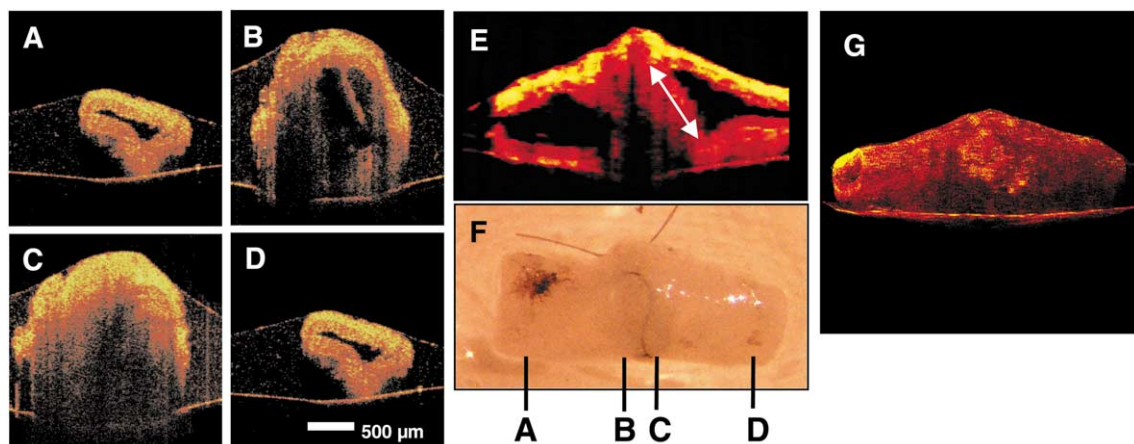


**Figure 7.** OCT images of an anastomosis in a rabbit artery. The 1 mm diameter rabbit artery was anastomosed with a continuous suture as seen in en face image (F). The lines indicate the OCT imaging planes. (A,D) Opposite ends of the anastomosis showing multi-layered structure of the artery with a patent lumen. (B) Partially obstructed lumen and the presence of a thrombotic flap. (C) Fully obstructed portion of the anastomosis site. (G) Three-dimensional projections can be constructed from arbitrary viewpoints. From [37]: Boppart S.A. et al., Intraoperative assessment of microsurgery with three-dimensional optical coherence tomography, *Radiology* 208 (1998) 81–86.

easily integrated with surgical microscopes. Hand held OCT surgical probes and laparoscopes have also been demonstrated [38]. One example of a surgical application for OCT is the repair of small vessels and nerves following traumatic injury. A technique capable of real-time, subsurface, three-dimensional, micron-scale imaging would permit the intraoperative monitoring of microsurgical procedures, giving immediate feedback to the surgeon that could enable difficult procedures and improve outcome. *Figure 7* shows in vitro OCT images of an arterial anastomosis of a rabbit inguinal artery demonstrating the ability of OCT to assess internal structure and luminal patency. An artery segment was bisected cross-sectionally with a scalpel and then re-anastomosed. A series of 40 cross-sectional images was acquired perpendicular to the long axis at 100  $\mu\text{m}$  spacing. The specimen was also digitally imaged with a CCD camera. Cross-sectional OCT images ( $2.2 \times 2.2 \text{ mm}$ ,  $250 \times 600 \text{ pixel}$ ) and 3D projections of a 1 mm diameter rabbit inguinal artery are shown. *Figures 7A–7D* show transverse images at different positions through the anastomosis. The images of the ends of the artery clearly show arterial morphology corresponding to the intimal, medial, and adventitial layers of the elastic artery. The image from the site of the anastomosis shows that the lumen was obstructed by a tissue flap. By assembling a series of cross-sectional 2D images, a 3D dataset was produced. Arbitrary planes can be selected and corresponding sections displayed. Three-dimensional projections of the arterial anastomosis are shown in *figure 7*. The three-dimensional views can show microstructural features which are not evident in single cross sectional images.

#### 4. Imaging delivery devices

Because OCT imaging technology is fiber optic based, it can be easily integrated with many standard medical diagnostic instruments to enable internal body imaging. Using fiber optics, small diameter transverse scanning catheter/endoscopes have been developed and demonstrated [39]. The catheter/endoscope consists of a single-mode optical fiber encased in a hollow rotating torque cable. At the distal end, the fiber is coupled to a GRIN lens and a micropism to direct the OCT beam radially, perpendicular to the axis of the catheter. The cable and distal optics are encased in a transparent housing. The OCT beam is scanned by rotating the cable to permit transluminal imaging in a radar-like pattern, cross sectionally through vessels or hollow organs. *Figure 8* shows a photograph of the prototype catheter. The catheter/endoscope has a diameter of 2.9 French or 1 mm, comparable to the size of a standard intravascular ultrasound catheter. This is small enough to allow imaging in a human coronary artery or imaging using the accessory port of a standard endoscope or bronchoscope.

The catheter-endoscope OCT system enables the acquisition of in vivo images of internal organ systems. In vivo imaging of the pulmonary, gastrointestinal, and urinary tracts as well as arterial imaging have been demonstrated in animals [26,40]. *Figure 9* shows an example of a catheter/endoscope OCT image

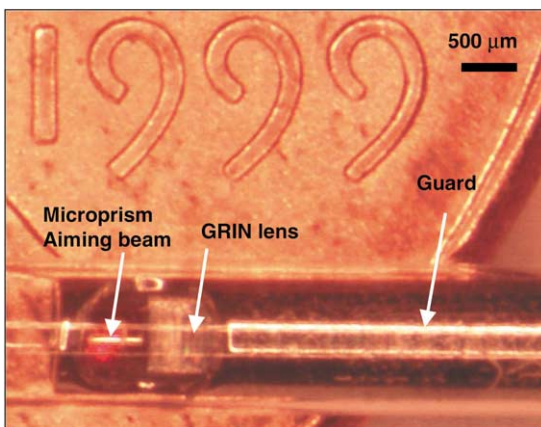


**Figure 8.** Photograph of prototype OCT catheter for transverse, intraluminal imaging. A single-mode fiber lies within a rotating flexible speedometer cable enclosed in a protective plastic sheath. The distal end focuses the beam at 90 degrees from the axis of the catheter. The diameter of the catheter was 1 mm.

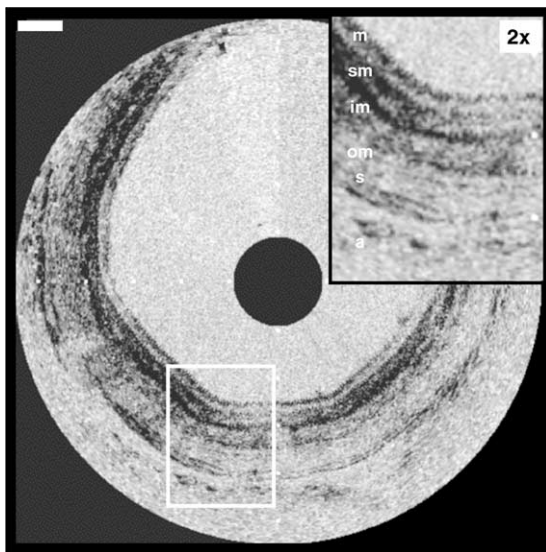


**Figure 9.** OCT catheter/endoscope image in vivo of the esophagus of a New Zealand white rabbit. The image clearly differentiates the layers of the esophagus including the mucosa, submucosa, inner muscularis, and outer muscularis. Reprinted with permission from [26]: Tearney G.J. et al., In vivo endoscopic optical biopsy with optical coherence tomography, *Science* 276 (1997) 2037–2039.

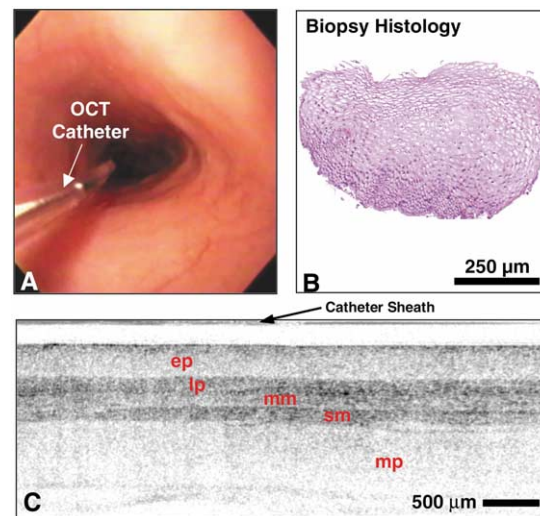


**Figure 10.** Clinical endoscopic OCT imaging of normal esophagus using linear scanning. (A) Endoscopic video image of normal region. (B) Biopsy histology of normal squamous epithelium. (C) OCT image of normal squamous epithelium with relatively uniform and distinct layered structures. From [41]: Li X.D. et al., Optical coherence tomography: advanced technology for the endoscopic imaging of Barrett's esophagus, *Endoscopy* 32 (2000) 921–930.

of the rabbit gastrointestinal tract. Imaging could be performed with either 256 or 512 lateral pixels, corresponding to image acquisition times of 125 ms or 250 ms, respectively. The two-dimensional image data were displayed using a polar coordinate transformation and inverse gray scale. OCT images of the in vivo rabbit esophagus permitted differentiation of the layers of the esophageal wall. The mucosa was readily identifiable because of its low optical backscattering compared with the submucosa.

Endoscopic OCT imaging in humans can be performed by introducing OCT imaging probes into the accessory port of standard endoscopes. *Figure 10* shows an example of endoscopic OCT imaging of the human esophagus [41]. Imaging was performing with 13 µm resolution at 1.3 µm wavelengths. These images show a representative linear scan OCT image, an endoscopic video image, and biopsy histology of normal squamous epithelium. The OCT image (4 mm × 2.5 mm, 512 × 256 pixels) of normal epithelium illustrates the relatively homogeneous epithelium (ep), the high-backscattering region (appears darker) of the lamina propria (lp), the low-backscattering muscularis mucosa (mm), the high-backscattering submucosa (sm), and the low-backscattering and thick muscularis propria (mp).

These studies demonstrate the feasibility of performing OCT imaging of internal organ systems and suggest the range of future clinical applications. Endoscopic OCT imaging studies in patients have been reported [32,34,41,42]. Numerous research groups are performing OCT imaging studies in patients for a wide range of clinical applications.

## 5. Ultrahigh resolution optical coherence tomography

The use of ultrashort pulse laser technology enables OCT imaging at unprecedented resolutions. The axial resolution is governed by the coherence length of the light source and is inversely proportional to the

optical bandwidth. Superluminescent diodes (SLDs) are often used for OCT imaging and typically have 10–15  $\mu\text{m}$  axial resolutions. In biomedical applications, this level of resolution is sufficient to image the architectural morphology or glandular organization of tissues, but is insufficient to image individual cells or subcellular structures such as nuclei. Cellular level resolution is important for detecting early neoplastic (cancerous) changes as well as for applications in biological microscopy. Ultrahigh resolution OCT would also improve sensitivity and specificity of diagnosis for ophthalmic diseases. Previous investigators have used broadband fluorescence from an organic dye and from  $\text{Ti}:\text{Al}_2\text{O}_3$  to achieve resolutions of  $\sim 2 \mu\text{m}$  in low coherence interferometry; however, OCT imaging was not possible because these sources have low power [43,44]. With the development of femtosecond Kerr lens modelocked (KLM) lasers which can generate low-coherence light with high single-mode powers, high-resolution and high-speed OCT imaging became possible [45–47].

State of the art femtosecond  $\text{Ti}:\text{Al}_2\text{O}_3$  lasers can now directly generate pulse durations of  $\sim 5 \text{ fs}$  [48–50]. These pulse durations correspond to only two optical cycles and have bandwidths of up to 400 nm centered around 800 nm. These high performance lasers have been made possible through the development of double-chirped mirror technology, which yields extremely wide bandwidths and also compensates higher-order dispersion in the laser. Unlike ultrafast femtosecond time resolved measurements, where special care must be exercised to maintain the short pulse duration, OCT measurements depend on field correlations rather than intensity correlations. Thus, dispersion in the reference and signal paths of the interferometer must be precisely matched, but need not be equal to zero. Field correlation is preserved even if the pulse duration is long. Thus OCT systems can be implemented fiber optically. Image resolutions of  $\sim 1 \mu\text{m}$  in biological tissues have been achieved [51].

*Figure 11* shows an example of an ultrahigh resolution OCT image of the retina of a normal human subject [52]. The axial resolution is 3  $\mu\text{m}$  and is by limited chromatic aberration in the eye. Comparison to standard resolution OCT imaging, *figure 4*, shows that ultrahigh resolution provides a significantly improved image quality with the ability to resolve internal retinal architectural morphology that is difficult to observe at lower resolutions. Cellular level OCT imaging can also be performed [47,51]. *Figure 12* shows an example of imaging of a *Xenopus laevis* tadpole (African frog). Imaging was performed with  $\sim 1 \mu\text{m}$  axial resolution and 3  $\mu\text{m}$  transverse resolution. Depth of field limitations may be overcome by using a novel technique from ultrasound known as C mode imaging. Multiple images are acquired with the focusing set to different depths within the specimen. Each image is in focus over a depth range comparable to the confocal parameter. The in-focus regions from each of the images are selected and fused together to form a single image, which has a greatly extended depth of field. The fused image covers an area of  $0.75 \times 0.5 \text{ mm}$  and consists of  $1700 \times 1000$  pixels. Because of the small focal spot size, the confocal parameter was only 40  $\mu\text{m}$ ; however, using image fusion of eight images enabled imaging over a depth of 750  $\mu\text{m}$ . Because

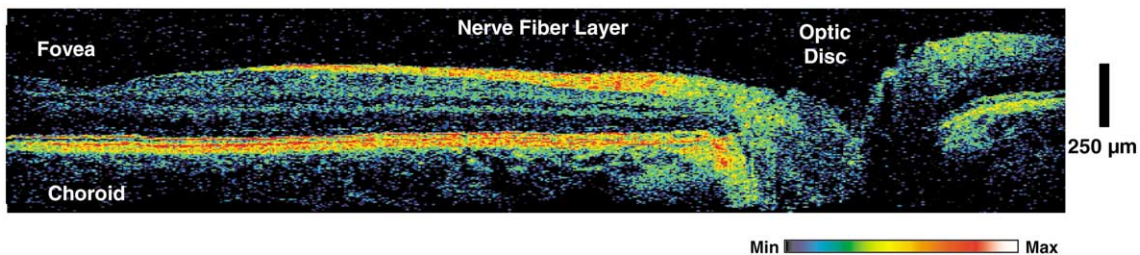
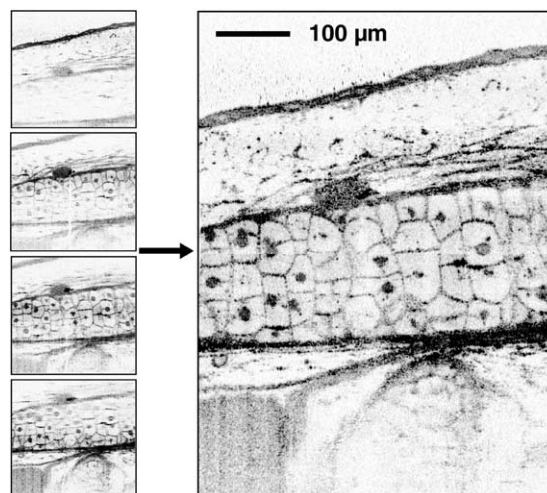


**Figure 11.** Ultrahigh-resolution retinal image along the axis between the optic disc and macula. The axial resolution is 3  $\mu\text{m}$  and the image has  $600 \times 725$  pixels. The image has been expanded by a factor of two in the axial direction in order to better visualize retinal structure. The nerve fiber layer is well differentiated and varies in thickness between the fovea and optic disc. From [52]: Drexler W. et al., Ultrahigh resolution ophthalmic optical coherence tomography, *Nature Med.* 7 (2001) 502–507.

**Figure 12.** Ultrahigh resolution imaging of *Xenopus laevis*. In vivo subcellular level resolution ( $1 \times 3 \mu\text{m}$ , longitudinal  $\times$  transverse,  $1700 \times 1000$  pixels) image of an African frog tadpole (*Xenopus laevis*). Images were recorded with different depths of focus and fused to construct the image shown. Multiple mesenchymal cells of various sizes and nuclear-to-cytoplasmic ratios and intracellular morphology, as well as the mitosis of cell pairs, are clearly shown. The bar is  $100 \mu\text{m}$ . From [51]: Drexler W. et al., In vivo ultrahigh resolution optical coherence tomography, *Opt. Lett.* 24 (1999) 1221–1223.



the axial and transverse resolutions are extremely fine, images have large pixel densities. Images can be beyond the resolution of a standard computer monitor and need to be viewed with panning and zooming. These OCT images show in vivo subcellular features.

### Summary

OCT can perform optical biopsy, the micron scale imaging of tissue morphology in situ and in real time. Image information is available in real time without the need for excision and histological processing of a specimen. The development of high-resolution and high-speed OCT technology as well as OCT compatible catheter/endoscopes and other delivery systems, represents enabling steps for many future OCT imaging clinical applications. More research remains to be done and numerous clinical studies must be performed in order to determine in which clinical situations OCT can play a role. However, the unique capabilities of OCT imaging suggest that it has the potential to have a significant impact on the diagnosis and clinical management of many diseases.

**Acknowledgements.** The scientific contributions of Mark Brezinski, Xingde Li, Wolfgang Drexler, Ingmar Hartl, Christian Chudoba, Pei-Lin Hsiung, Tony Ko, Stephen Boppart, Joel Schuman, Carmen Puliafito, Costas Pitris, Brett Bouma, and Gary Tearney, are gratefully acknowledged. This research is supported in part by the National Institutes of Health, Contracts NIH-9-RO1-CA75289-04, NIH-9-RO1-EY11289-15, NIH-RO1-AR44812-04, NIH-1-R29-HL55686-01A1, the Office of Naval Research Medical Free Electron Laser Program, Contract N000014-97-1-1066, and the Whittaker Foundation Contract 96-0205.

### References

- [1] Huang D., Swanson E.A., Lin C.P., Schuman J.S., Stinson W.G., Chang W., Hee M.R., Flotte T., Gregory K., Puliafito C.A., Fujimoto J.G., Optical coherence tomography, *Science* 254 (1991) 1178–1181.
- [2] Fujimoto J.G., Brezinski M.E., Tearney G.J., Boppart S.A., Bouma B., Hee M.R., Southern J.F., Swanson E.A., Optical biopsy and imaging using optical coherence tomography, *Nature Med.* 1 (1995) 970–972.
- [3] Brezinski M.E., Fujimoto J.G., Optical coherence tomography: high resolution imaging in nontransparent tissue, *IEEE J. Sel. Topics Quant. Electron.* 5 (4) (1999) 1185–1192.
- [4] Fujimoto J.G., Pitris C., Boppart S.A., Brezinski M.E., Optical coherence tomography: an emerging technology for biomedical imaging and optical biopsy, *Neoplasia* 2 (2000) 9–25.
- [5] Takada K., Yokohama I., Chida K., Noda J., New measurement system for fault location in optical waveguide devices based on an interferometric technique, *Appl. Opt.* 26 (1987) 1603–1608.
- [6] Youngquist R.C., Carr S., Davies D.E.N., Optical coherence-domain reflectometry: a new optical evaluation technique, *Opt. Lett.* 12 (1987) 158–160.

- [7] Gilgen H.H., Novak R.P., Salathe R.P., Hodel W., Beaud P., Submillimeter optical reflectometry, *IEEE J. Lightwave Technol.* 7 (1989) 1225–1233.
- [8] Fercher A.F., Mengedocht K., Werner W., Eye-length measurement by interferometry with partially coherent light, *Opt. Lett.* 13 (1988) 1867–1869.
- [9] Huang D., Wang J., Lin C.P., Puliafito C.A., Fujimoto J.G., Micron-resolution ranging of cornea and anterior chamber by optical reflectometry, *Lasers Surgery Med.* 11 (1991) 419–425.
- [10] Swanson E.A., Izatt J.A., Hee M.R., Huang D., Lin C.P., Schuman J.S., Puliafito C.A., Fujimoto J.G., In vivo retinal imaging by optical coherence tomography, *Opt. Lett.* 18 (1993) 1864–1866.
- [11] Fercher A.F., Hitztenberger C.K., Drexler W., Kamp G., Sattmann H., In vivo optical coherence tomography, *Am. J. Ophthalmol.* 116 (1993) 113–114.
- [12] Hee M.R., Izatt J.A., Swanson E.A., Huang D., Lin C.P., Schuman J.S., Puliafito C.A., Fujimoto J.G., Optical coherence tomography of the human retina, *Arch. Ophthalmol.* 113 (1995) 325–332.
- [13] Puliafito C.A., Hee M.R., Lin C.P., Reichel E., Schuman J.S., Duker J.S., Izatt J.A., Swanson E.A., Fujimoto J.G., Imaging of macular diseases with optical coherence tomography, *Ophthalmology* 102 (1995) 217–229.
- [14] Hee M.R., Puliafito C.A., Wong C., Duker J.S., Reichel E., Schuman J.S., Swanson E.A., Fujimoto J.G., Optical coherence tomography of macular holes, *Ophthalmology* 102 (1995) 748–756.
- [15] Hee M.R., Izatt J.A., Swanson E.A., Huang D., Schuman J.S., Lin C.P., Puliafito C.A., Fujimoto J.G., Optical coherence tomography for ophthalmic imaging: new technique delivers micron-scale resolution, *IEEE Eng. Med. Biol.* 14 (1995) 67–76.
- [16] Schuman J.S., Hee M.R., Puliafito C.A., Wong C., Pedut-Kloizman T., Lin C.P., Hertzmark E., Izatt J.A., Swanson E.A., Fujimoto J.G., Quantification of nerve fiber layer thickness in normal and glaucomatous eyes using optical coherence tomography, *Arch. Ophthalmol.* 113 (1995) 586–596.
- [17] Schuman J.S., Noecker R.J., Imaging of the optic nerve head and nerve fiber layer in glaucoma, *Ophthalmol. Clin. North Amer.* 8 (1995) 259–279.
- [18] Puliafito C.A., Hee M.R., Schuman J.S., Fujimoto J.G., *Optical Coherence Tomography of Ocular Diseases*, Slack, Thorofare, NJ, 1996.
- [19] Hee M.R., Bauman C.R., Puliafito C.A., Duker J.S., Reichel E., Wilkins J.R., Coker J.G., Schuman J.S., Swanson E.A., Fujimoto J.G., Optical coherence tomography of age-related macular degeneration and choroidal neovascularization, *Ophthalmology* 103 (1996) 1260–1270.
- [20] Hee M.R., Puliafito C.A., Duker J.S., Reichel E., Coker J.G., Wilkins J.R., Schuman J.S., Swanson E.A., Fujimoto J.G., Topography of diabetic macular edema with optical coherence tomography, *Ophthalmology* 105 (1998) 360–370.
- [21] Schmitt J.M., Knuttel A., Yadlowsky M., Eckhaus M.A., Optical coherence tomography of a dense tissue – statistics of attenuation and backscattering, *Phys. Med. Biol.* 39 (1994) 1705–1720.
- [22] Schmitt J.M., Yadlowsky M., Bonner R.F., Subsurface imaging of living skin with optical coherence tomography, *Dermatology* 191 (1995) 93–98.
- [23] Brezinski M.E., Tearney G.J., Bouma B.E., Izatt J.A., Hee M.R., Swanson E.A., Southern J.F., Fujimoto J.G., Optical coherence tomography for optical biopsy: properties and demonstration of vascular pathology, *Circulation* 93 (1996) 1206–1213.
- [24] Brezinski M.E., Tearney G.J., Weissman N.J., Boppart S.A., Bouma B.E., Hee M.R., Weyman A.E., Swanson E.A., Southern J.F., Fujimoto J.G., Assessing atherosclerotic plaque morphology: Comparison of optical coherence tomography and high frequency intravascular ultrasound, *British Heart J.* 77 (1997) 397–404.
- [25] Tearney G.J., Brezinski M.E., Southern J.F., Bouma B.E., Boppart S.A., Fujimoto J.G., Optical biopsy in human gastrointestinal tissue using optical coherence tomography, *Am. J. Gastroent.* 92 (1997) 1800–1804.
- [26] Tearney G.J., Brezinski M.E., Bouma B.E., Boppart S.A., Pitris C., Southern J.F., Fujimoto J.G., In vivo endoscopic optical biopsy with optical coherence tomography, *Science* 276 (1997) 2037–2039.
- [27] Tearney G.J., Brezinski M.E., Southern J.F., Bouma B.E., Boppart S.A., Fujimoto J.G., Optical biopsy in human urologic tissue using optical coherence tomography, *J. Urol.* 157 (1997) 1915–1919.
- [28] Tearney G.J., Brezinski M.E., Southern J.F., Bouma B.E., Boppart S.A., Fujimoto J.G., Optical biopsy in human pancreatobiliary tissue using optical coherence tomography, *Dig. Dis. Sci.* 43 (1998) 1193–1199.
- [29] Pitris C., Brezinski M.E., Bouma B.E., Tearney G.J., Southern J.F., Fujimoto J.G., High resolution imaging of the upper respiratory tract with optical coherence tomography – A feasibility study, *Am. J. Respir. Crit. Care Med.* 157 (1998) 1640–1644.
- [30] Pitris C., Goodman A., Boppart S.A., Libus J.J., Fujimoto J.G., Brezinski M.E., High-resolution imaging of gynecologic neoplasms using optical coherence tomography, *Obstet. Gynecol.* 93 (1999) 135–139.
- [31] Jesser C.A., Boppart S.A., Pitris C., Stamper D.L., Nielsen G.P., Brezinski M.E., Fujimoto J.G., High resolution endoscopic evaluation of transitional cell carcinoma with optical coherence tomography, *British J. Radiol.* 72 (1999) 1170–1176.

- [32] Rollins A.M., Ung-Arunyawee R., Chak A., Wong C.K., Kobayashi K., Sivak M.V., Izatt J.A., Real-time in vivo imaging of human gastrointestinal ultrastructure by use of endoscopic optical coherence tomography with a novel efficient interferometer design, *Opt. Lett.* 24 (1999) 1358–1360.
- [33] Pitris C., Jessor C., Boppart S.A., Stamper D., Brezinski M.E., Fujimoto J.G., Feasibility of optical coherence tomography for high resolution imaging of human gastrointestinal tract malignancies, *J. Gastroent.* 35 (2000) 87–92.
- [34] Bouma B.E., Tearney G.J., Compton C.C., Nishioka N.S., High-resolution imaging of the human esophagus and stomach in vivo using optical coherence tomography, *Gastroint. Endosc.* 51 (2000) 467–474.
- [35] Brezinski M.E., Tearney G.J., Boppart S.A., Swanson E.A., Southern J.F., Fujimoto J.G., Optical biopsy with optical coherence tomography, feasibility for surgical diagnostics, *J. Surg. Res.* 71 (1997) 32–40.
- [36] Boppart S.A., Brezinski M.E., Pitris C., Fujimoto J.G., Optical coherence tomography for neurosurgical imaging of human intracortical melanoma, *Neurosurgery* 43 (1998) 834–841.
- [37] Boppart S.A., Bouma B.E., Pitris C., Southern J.F., Brezinski M.E., Fujimoto J.G., Intraoperative assessment of microsurgery with three-dimensional optical coherence tomography, *Radiology* 208 (1998) 81–86.
- [38] Boppart S.A., Bouma B.E., Pitris C., Tearney G.J., Fujimoto J.G., Brezinski M.E., Forward-imaging instruments for optical coherence tomography, *Opt. Lett.* 22 (1997) 1618–1620.
- [39] Tearney G.J., Boppart S.A., Bouma B.E., Brezinski M.E., Weissman N.J., Southern J.F., Fujimoto J.G., Scanning single mode catheter/endoscope for optical coherence tomography, *Opt. Lett.* 21 (1996) 543–545.
- [40] Fujimoto J.G., Boppart S.A., Tearney G.J., Bouma B.E., Pitris C., Brezinski M.E., High resolution in vivo intra-arterial imaging with optical coherence tomography, *Heart* 82 (1999) 128–133.
- [41] Li X.D., Boppart S.A., Van Dam J., Mashimo H., Mutinga M., Drexler W., Klein M., Pitris C., Krinsky M.L., Brezinski M.E., Fujimoto J.G., Optical coherence tomography: advanced technology for the endoscopic imaging of Barrett's esophagus, *Endoscopy* 32 (2000) 921–930.
- [42] Sergeev A.M., Gelikonov V.M., Gelikonov G.V., Feldchtein F.I., Kuranov R.V., Gladkova N.D., Shakhova N.M., Snopova L.B., Shakov A.V., Kuznetzova I.A., Denisenko A.N., Pochinko V.V., Chumakov Y.P., Streltzova O.S., In vivo endoscopic OCT imaging of precancer and cancer states of human mucosa, *Opt. Express* 1 (1997) 432.
- [43] Liu H.H., Cheng P.H., Wang J., Spatially coherent white light interferometer based on a point fluorescent source, *Opt. Lett.* 18 (1993) 678–680.
- [44] Clivaz X., Marquis-Weible F., Salathe R.P., Optical low coherence reflectometry with 1.9  $\mu\text{m}$  spatial resolution, *Electron. Lett.* 28 (1992) 1553–1554.
- [45] Bouma B., Tearney G.J., Boppart S.A., Hee M.R., Brezinski M.E., Fujimoto J.G., High-resolution optical coherence tomographic imaging using a mode-locked Ti-Al<sub>2</sub>O<sub>3</sub> laser source, *Opt. Lett.* 20 (1995) 1486–1488.
- [46] Bouma B.E., Tearney G.J., Bilinsky I.P., Golubovic B., Self phase modulated Kerr-lens mode locked Cr:forsterite laser source for optical coherent tomography, *Opt. Lett.* 21 (1996) 1839–1841.
- [47] Boppart S.A., Bouma B.E., Pitris C., Southern J.F., Brezinski M.E., Fujimoto J.G., In vivo cellular optical coherence tomography imaging, *Nature Med.* 4 (1998) 861–865.
- [48] Morgner U., Kärtner F.X., Cho S.H., Chen Y., Haus H.A., Fujimoto J.G., Ippen E.P., Scheuer V., Angelow G., Tschudi T., Sub-two-cycle pulses from a Kerr-lens mode-locked Ti:sapphire laser, *Opt. Lett.* 24 (1999) 411–413.
- [49] Sutter D.H., Steinmeyer G., Gallmann L., Matuschek N., Morier-Genoud F., Keller U., Scheuer V., Angelow G., Tschudi T., Semiconductor saturable-absorber mirror assisted Kerr-lens mode-locked Ti:sapphire laser producing pulses in the two-cycle regime, *Opt. Lett.* 24 (1999) 631–633.
- [50] Ell R., Morgner U., Kärtner F.X., Fujimoto J.G., Ippen E.P., Scheuer V., Angelow G., Tschudi T., Generation of 5 fs pulses and octave-spanning spectra directly from a Ti:sapphire laser, *Opt. Lett.* (2001), in press.
- [51] Drexler W., Morgner U., Kaertner F.X., Pitris C., Boppart S.A., Li X.D., Ippen E.P., Fujimoto J.G., In vivo ultrahigh resolution optical coherence tomography, *Opt. Lett.* 24 (1999) 1221–1223.
- [52] Drexler W., Morgner U., Ghanta R.K., Kärtner F.X., Schuman J.S., Fujimoto J.G., Ultrahigh resolution ophthalmic optical coherence tomography, *Nature Med.* 7 (2001) 502–507.